Am J Cancer Res 2019;9(7):1439-1453
www.ajcr.us /ISSN:2156-6976/ajcr0097931

*Original Article*

# Monocyte recruitment and activated inflammation are associated with thyroid carcinogenesis in a mouse model

Sunmi Park[1], Jack Zhu[2], Grégoire Altan-Bonnet[3], Sheue-Yann Cheng[1]

*[1]Laboratory of Molecular Biology, [2]Cancer Genetics Branch, [3]Immunodynamics Group, Cancer and Inflammation Program, Center for Cancer Research, National Cancer Institute, Bethesda, Maryland 20892-4264, USA*

Received June 3, 2019; Accepted June 10, 2019; Epub July 1, 2019; Published July 15, 2019

**Abstract:** Thyroid cancer is the most common endocrine malignancy. Although an association between inflammation and thyroid cancer has long been recognized, a cause-effect relationship at the molecular level has yet to be elucidated. We explored how inflammation could contribute to thyroid carcinogenesis in *Thrb*$^{PV/PV}$*Pten*$^{+/-}$ mice. The *Thrb*$^{PV/PV}$*Pten*$^{+/-}$ mouse expresses a dominantly negative thyroid hormone receptor β (denoted as PV) and a deletion of one single allele of the Pten gene. This mutant mouse exhibits aggressive follicular thyroid cancer similarly as in patients. We found significantly increased infiltration of inflammatory monocytes in thyroid tumors of *Thrb*$^{PV/PV}$*Pten*$^{+/-}$ mice, while no apparent changes in monocyte homeostasis in the bone marrow and blood of tumor-bearing mice. Using global gene expression profiling, we found altered expression of inflammation mediators in that the expression of Ptgs1, Sphk1, OPN, Chil1, Tnfrsf18, IL6, and Ccl12 genes was significantly increased and expression of Kit, Ly96, Ephx2, CD163, IL15, and Ccr2 was significantly decreased. Subsequent validation of the gene expression by mRNA analysis prompted us to further delineate the inflammatory role of osteopontin (OPN) in thyroid carcinogenesis because of its critical role in monocyte/macrophage functions and proinflammatory responses. We found that the protein abundance of OPN and its receptor, integrin β1, was highly increased and, concurrently, the downstream effectors AKT and NF-κB were significantly elevated to drive thyroid tumor progression of *Thrb*$^{PV/PV}$*Pten*$^{+/-}$ mice. These results demonstrated that increased inflammation driven by elevated expression of immune-related genes and cytokines promoted thyroid cancer progression. Importantly, we uncovered OPN as a novel regulator in inflammatory response during thyroid carcinogenesis. These preclinical findings suggested that OPN can be a potential target for thyroid cancer therapy via modulation of inflammatory signaling.

**Keywords:** Inflammation, activated monocytes, thyroid cancer, cDNA microarrays, apoptosis, AKT signaling, osteopontin, integrins

## Introduction

Thyroid cancer is the most common endocrine malignancy and its incidence is rapidly increasing worldwide. There are three major types: well-differentiated thyroid cancer (WDTC) including the papillary and follicular histological types, poorly differentiated thyroid cancer (PDTC), and anaplastic thyroid cancer (ATC). The prognosis of WDTC is good, with a 10-year survival rate of 90-95%. For PDTC and ATC, the prognosis is poor, especially for patients ATC who rarely survive beyond 1 year from the time of diagnosis. Intensive efforts in the past decades have identified many genetic lesions in de-differentiated and anaplastic thyroid cancer. Some of the identified molecular targets were tested in patients in clinical trials with some positive, though limited, outcomes. Recent technological advances in targeted next-generation sequencing have uncovered many novel genetic events previously not identified in PDTC and ATC [1, 2]. Some of the key players involved in the genetic alterations could eventually move forward to be tested for their treatment efficacy in patients with advanced thyroid cancer. However, regulators that play key roles in the tumor microenvironment to affect thyroid cancer progression (e.g., inflammation/immunity) that could also be consid-

ered as opportunity for potential novel treatment modality in thyroid cancer have been less explored. One possible reason is that the molecular basis underlying cause-effect of inflammation/immunity and thyroid cancer progression has not been fully elucidated.

Inflammation is a crucial function of the innate immune system that protects against pathogens and initiates specific immunity. Acute inflammation is a rapid and self-limiting process. However, either the abnormal persistence of the stimuli that induced the inflammatory response or the failure of the mechanisms that make it end results in chronic inflammation [3]. A relationship between chronic inflammation and cancer was first hypothesized by Virchow in the nineteenth century on the basis of observations that tumors often arose at sites of chronic inflammation and that inflammatory cells were present in biopsied samples from tumors [4]. Since then, epidemiological studies and animal models have demonstrated that cancer and inflammation are closely linked. Several human cancers arise from inflammatory responses due to infectious agents. Nonetheless, tumors without a microbial background could present signs of "smoldering inflammation" [5]. Key features of cancer-related inflammation include the infiltration of lymphocytes, prominently tumor-associated macrophages (TAMs), the presence of mediators and cellular effectors of inflammation. [Cytokines such as tumor necrosis factor (TNF), interleukin (IL)-1, IL-6; chemokines such as CCL2 and CXCL8; prostaglandins such as Cox2 and ptgs1], and the occurrence of tissue remodeling and angiogenesis [5, 6].

Evidence for an association of WDTC with inflammation comes from observations that a mixture of immune cells frequently is found within primary thyroid tumors [7-10]. Yet, the role of immune-inflammatory responses in thyroid carcinogenesis has been debated. One study reported that advanced thyroid cancers such as PDTC and ATC have less lymphocytic cell and dendritic cell filtration than PTC, suggesting infiltrated lymphocytes and dendritic cells could be protective in thyroid cancer [11]. Other studies, however, reported that immune cells such as TAMs are pro-tumorigenic in that increased TAM infiltration in PDTC was positively correlated with capsular invasion, extrathyroidal extension, and poor prognosis [12]. Further, interconnected TAMs closely intermingled with cancer cells were reported to be directly related with the aggressiveness of ATC [13]. Recently, transcriptome analysis by next-generation sequencing identified an enrichment of M2 macrophage gene signatures with patient-derived ATC tumors, further supporting the pro-tumorigenic role of TAMs [1]. Even so, molecular changes in immune-inflammatory responses during thyroid cancer progression have yet to be fully elucidated.

In the present studies, we aimed to identify the altered immune-inflammatory responses at the molecular level during thyroid cancer progression by using a mouse model (*Thrb*$^{PV/PV}$*Pten*$^{+/-}$ mice). The *Thrb*$^{PV/PV}$*Pten*$^{+/-}$ mouse expresses a potent dominantly negative thyroid hormone receptor β (TRβPV) with a deletion of one allele of the *Pten* gene. This *Thrb*$^{PV/PV}$*Pten*$^{+/-}$ mouse has previously been shown to fully recapitulate human follicular thyroid cancer [14] and has been used as a preclinical model for testing potential molecular targets [15, 16]. Using global gene expression profiling, we identified altered expression of a large number of inflammation-related genes during thyroid carcinogenesis, demonstrating that increased inflammation driven by elevated expression of immune-related genes and cytokines promoted thyroid cancer progression. Further in-depth analysis showed pathways initiated from osteopontin (OPN) play key roles in affecting immune-responses during cancer development, suggesting that OPN can be a potential target for thyroid cancer therapy via modulation of immune-inflammatory signaling.

## Materials and methods

### *Mice*

Animal protocols for care and handling in the present study were approved by the National Cancer Institute Animal Care and Use Committee. Generation of *Thrb*$^{PV/PV}$*Pten*$^{+/-}$ mice was described in previous studies [14].

### *RNA quality analysis and microarray*

Total RNA from thyroid tissues was isolated using Trizol (Thermo Fisher Scientific, Waltham, MA). Quality of RNA was confirmed with the Agilent RNA 6000 Nano Kit (Agilent Technologies, Santa Clara, CA). Total RNA was used

for the expression analysis using Affymetrix Clariom S arrays (Thermo-Fisher, Grand Island, NY) according to the manufacturer's protocol. The Cancer Genome Atlas (TCGA) data were downloaded from Firebrowse (http://firebrowse.org/).

*RNA extraction and RT-qPCR*

Total RNA was isolated from thyroid tissues using Trizol (Thermo Fisher Scientific, Waltham, MA). RT-qPCR was performed with one step SYBR Green RT-qPCR Master Mix (Qiagen, Valencia, CA). The mRNA level of each gene was normalized to the GAPDH (glyceraldehyde-3-phosphate dehydrogenase) mRNA level. The primer sequences are listed in Table S1.

*Western blot analysis*

Western blot analysis from thyroid tissues was carried as described previously [16]. 30 μg of protein sample was loaded and separated for the analysis. Primary antibodies for OPN (1:1000 dilution) and NF-κB p65 (1:1000) were purchased from abcam (Cambridge, MA). p-AKT (1:1000 dilution), total-AKT (1:2000 dilution), and p-BAD (1:500 dilution) were purchased from Cell Signaling Technology (Danvers, MA). Antibodies for Integrin β1 (1:1000 dilution), Cox2 (1:500 dilution), TGF-β1 (1:500 dilution), and TNF-α (1:500 dilution) were purchased from Santa Cruz Biotechnology (Dallas, TX). F4/80 antibody (1:500 dilution) was purchased from Thermo Fisher Scientific (Waltham, MA). β-Actin antibody was purchased from (Sigma-Aldrich, St. Louis, MO). Band intensities were quantified by using NIH IMAGE software (Image J 1.48v).

*Histopathologic analysis and immunohistochemistry*

Thyroid gland was fixed in 10% neutral-buffered formalin (NBF, approximately 4% formaldehyde) (Sigma-Aldrich, St. Louis, MO) and subsequently embedded in paraffin. 5-μm-thickn sections were stained with hematoxylin and eosin (HistoServ, Germantown, MD). Immunohistochemistry (IHC) was conducted similarly as described [17]. Primary antibodies for OPN (1:300 dilution) and NF-κB p65 (1:500 dilution) were purchased from abcam (Cambridge, MA). F4/80 (1:200 dilution) antibody was purchased from Thermo Fisher Scientific (Waltham, MA) for immunohistochemistry. A primary antibody was incubated with tissue section overnight at 4°C. Peroxidase activity from the secondary antibody was developed with diaminobenzidine (DAB). And the sections were counterstained with hematoxylin.

*Flow cytometry analysis*

The sources of antibodies and fluorophore-labeled antibodies used in FACS analyses are listed in Table S2. Blood samples were collected and their red blood cells were lysed using an ACK lysis buffer (Quality Biological, Gaithersburg MD). Cells were also isolated from thyroid tissues and prepared as a single-cell suspension by physical dissociation. Single-cell suspensions were first incubated with Fc receptor blocking Abs (CD16/CD32, Thermo Fisher Scientific, Waltham, MA) for 15 min on ice and incubated for 30 min with indicated mouse antibodies on ice and washed with PBS + 2% BSA buffer. Stained cells were analyzed using a BD Fortessa II flow cytometer (BD Biosciences, San Jose, CA). FACS measurements were compensated and analyzed using FlowJo, LLC (Tree Star Inc, Ashland, OR).

*Statistical analysis*

All statistical analyses and the graphs were performed and generated using GraphPad Prism version 7.0 (GraphPad Software, La Jolla, CA). $P<0.05$ is considered statistically significant. All data are expressed as mean ± SEM.

## Results

*Increased infiltration of inflammatory monocytes in thyroid tumors of $Thrb^{PV/PV}Pten^{+/-}$ mice*

We used $Thrb^{PV/PV}Pten^{+/-}$ mice as a preclinical model to study how inflammatory microenvironment changes impacted thyroid carcinogenesis. Our previous study showed that the 50% survival age of $Thrb^{PV/PV}Pten^{+/-}$ mice was at ~5.5 months [14]. Consistent with previous data, $Thrb^{PV/PV}Pten^{+/-}$ mice became moribund with signs of palpable tumors, rapid weight loss, hunched posture, and labored breathing after 4 months of age. Therefore, thyroid tissues in this study were collected from mice whose age was between 4 and ~6 months when mice were showing the above symptoms. Thyroid tumors in $Thrb^{PV/PV}Pten^{+/-}$ mice were significantly larger

than thyroid tissue of wild-type controls (**Figure 1A**, panel b versus panel a). Further, H&E staining showed that the histologic features were changed from normal thyroid follicular cells in wild-type mice to tumor phenotype in *Thrb*$^{PV/PV}$*Pten*$^{+/-}$ mice (**Figure 1A**, panel c versus panel d).

It is known that monocyte/macrophage lineage cells accumulate in the tumor microenvironment of many types of human and murine tumors and are thought to regulate tumor development [18]. Monocytes differentiate in the bone marrow and circulate throughout the body in responding to inflammation and infection. Therefore, we first examined the thyroid tissues of wild-type and *Thrb*$^{PV/PV}$*Pten*$^{+/-}$ mice using surface markers for the identification of the monocyte population. Monocytes are bone marrow-derived mononuclear phagocytes that circulate in the blood stream. In mice, circulating monocytes are classically defined by expression of CD115 (CSF1R), a receptor for the macrophage growth factor CSF1 (M-CSF) [19]. Accordingly, we gated the CD115$^+$-associated population in the leukocytes using single cell suspension from thyroid tissue of wild-type and *Thrb*$^{PV/PV}$*Pten*$^{+/-}$ mice. Monocytes can be divided in two main subsets in mice: Ly6C$^+$-inflammatory monocytes that are rapidly recruited to the site of inflammation, and Ly6C$^-$-monocytes that patrol the blood vessels [20]. In addition to two monocyte subsets, investigators have reported other subsets of monocytes expressing major histocompatibility complex class II (MHC II) and varying levels of Ly6C [21, 22]. We therefore first gated single cells from thyroid tissues of WT mice and *Thrb*$^{PV/PV}$*Pten*$^{+/-}$ mice: CD115$^+$Lineage$^-$(CD3-CD19-NKp46-Ter119-Ly6G-Sca1$^-$) from leukocyte population, followed by selection of matured monocytes using CD11b$^+$cKit$^-$. We found that thyroid tumor tissues were significantly infiltrated with monocytes (10.2% of CD11b$^+$cKit$^-$ cells in CD115$^+$Lin$^-$ population) while normal thyroids were essentially devoid of monocytes (1.7% of CD11b$^+$cKit$^-$ cells in CD115$^+$Lin$^-$ population). Since inflammatory monocytes were considered to have increased expression of MHC II [22, 23], we examined % inflammatory monocytes populated in Q2 + Q3 area of **Figure 1BI**, panels a and b. Quantitative graphing showed that inflammatory monocytes were increased by 7-fold in the thyroid tumors of *Thrb*$^{PV/PV}$*Pten*$^{+/-}$ *mice* compared with wild-type mice (**Figure 1BII**). These results indicate that monocytes with an inflammatory state had significantly infiltrated the thyroid tumor microenvironment of *Thrb*$^{PV/PV}$*Pten*$^{+/-}$ mice. Strikingly, we found that the distribution of monocytes in the blood (**Figure 1C**) and bone marrow (not shown) compartments were essentially identical for normal control and tumor-bearing mice. These findings strongly suggested that the thyroid tumor microenvironment sustains the elevation of inflammation in a compartmentalized and localized manner.

*Alterations in the global gene expression profiles in thyroid tumors of Thrb*$^{PV/PV}$*Pten*$^{+/-}$ *mice*

To examine altered expression of inflammation-related genes during thyroid carcinogenesis, we compared global gene expression profiles of thyroid tissues between wild-type and *Thrb*$^{PV/PV}$*Pten*$^{+/-}$ mice by using cDNA microarray analysis. Hierarchical clustering of the top 50 differentially expressed genes showed that expression patterns between wild-type and *Thrb*$^{PV/PV}$*Pten*$^{+/-}$ mice (**Figure 2A**). A total of 2,322 differentially expressed genes with changes more than 2-fold (with FDR <0.05; **Figure 2B**) were detected. Among these genes, 1,062 were up-regulated and 1,260 were down-regulated.

Additional functional enrichment analyses showed sixty-three inflammation-related genes were further classified based on KEGG pathway information. Pathway overrepresentation analysis highly ranked multiple genes related to cytokine-cytokine receptor interaction, chemokine signaling pathway, and NF-κB signaling pathway (**Figure 2C**). It is known that the hallmarks of cancer-related inflammation include the presence of inflammatory mediators such as chemokines, cytokines, and prostaglandins in tumor tissue. Accordingly, we selected top-ranking genes for further characterization. **Table 1** shows the down-regulated immune-related genes in thyroid tumors of *Thrb*$^{PV/PV}$*Pten*$^{+/-}$ mice compared with wild-type. The changes ranged from a high of 10.02-fold down to 2.06-fold. These genes are grouped into three categories in **Table 1**. In the inflammation-regulatory genes category, *kit, Ly96, CD163, and Ehpx2* were decreased in thyroid tumors of *Thrb*$^{PV/PV}$*Pten*$^{+/-}$ mice. In the interleukins and chemokines categories, interleukins (*il15* and *il18*), interleukin receptor and associ-

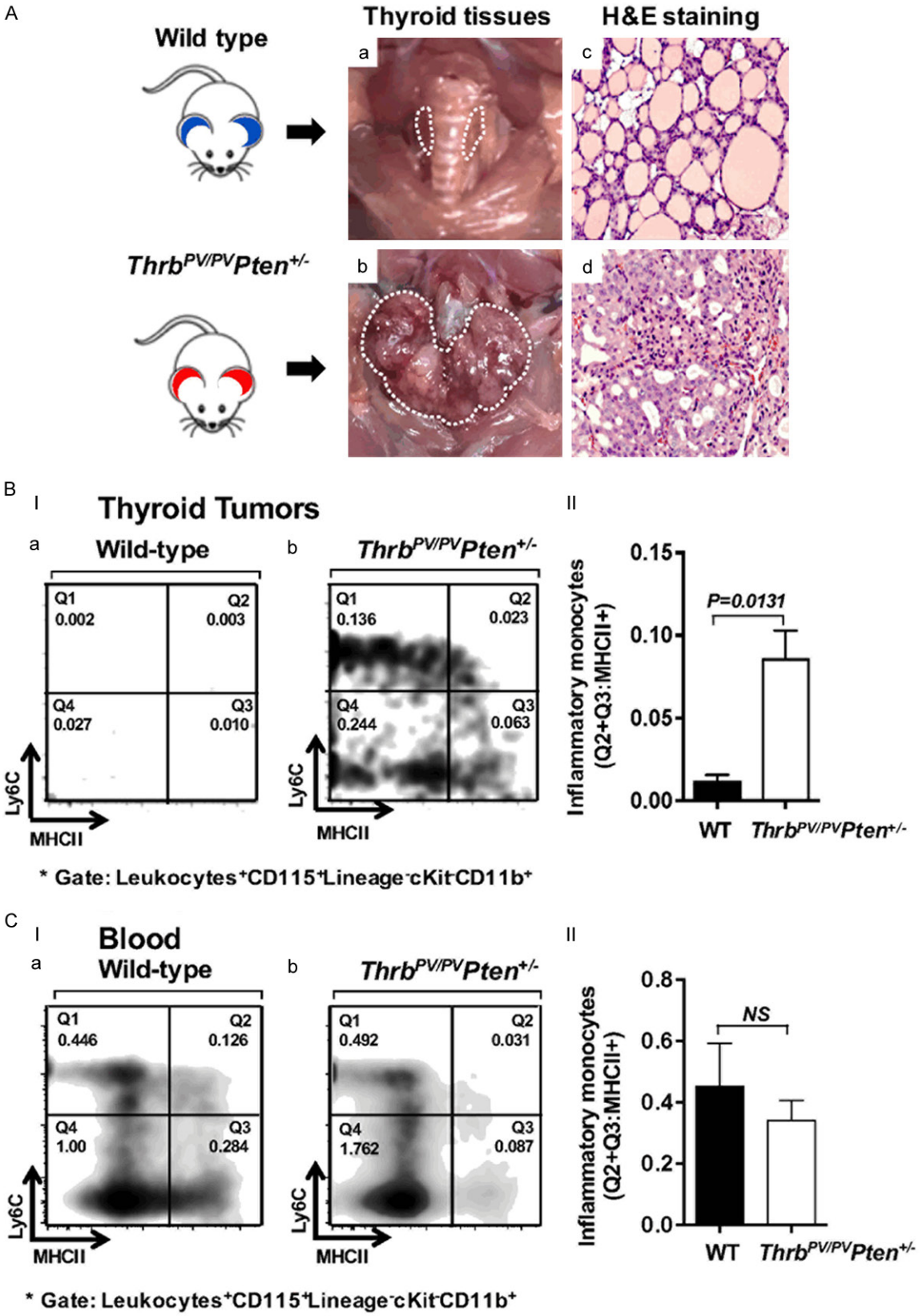


**Figure 1.** Increased inflammatory monocytes in thyroid tumors of *Thrb*$^{PV/PV}$*Pten*$^{+/-}$ mice. (A) Thyroid glands of wild-type (a) and *Thrb*$^{PV/PV}$*Pten*$^{+/-}$ (b) mice of the same age (from 4 to ~6 months) were dissected for H&E staining of thyroid tissues of wild-type mice (c) and *Thrb*$^{PV/PV}$*Pten*$^{+/-}$ mice (d). (BI) Analysis of monocyte population in the thyroid tissue of

wild-type (a) and *Thrb*$^{PV/PV}$*Pten*$^{+/-}$ (b) mice. Monocytes were analyzed by FACS using cell surface markers. Monocytes were identified cells in thyroid that had characteristics of leukocytes$^{+}$CD115$^{+}$lineage$^{-}$(CD3-CD19-NKp46-Ter119-LysG-Sca1-) cKit$^{-}$CD11b$^{+}$ population. Further analysis using Ly6C and MHCII antibodies yielded detailed classification of monocytes in the thyroid tissue of wild-type and *Thrb*$^{PV/PV}$*Pten*$^{+/-}$ mice. (BII) Quantification of % MHCII$^{+}$ inflammatory monocytes in the thyroid tissue of wild-type (n=20) and *Thrb*$^{PV/PV}$*Pten*$^{+/-}$ (n=8) mice. (CI) Analysis of monocyte population in the blood of wild-type (a) and *Thrb*$^{PV/PV}$*Pten*$^{+/-}$ (b) mice. Monocytes were analyzed by FACS using same procedure with (BI). (CII) Quantification of % MHCII$^{+}$ inflammatory monocytes in the blood of wild-type (n=5) and *Thrb*$^{PV/PV}$*Pten*$^{+/-}$ (n=3) mice. Values are means ± SEM. The *P* values are indicated.

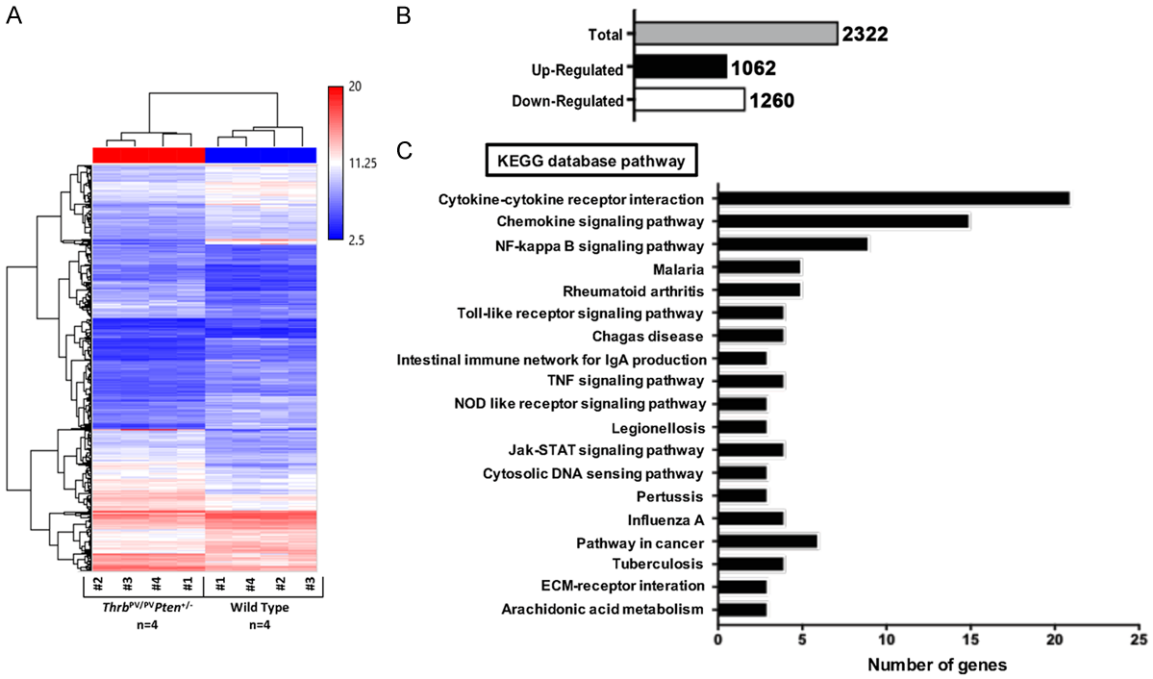


**Figure 2.** Comparison of gene expression profiles of thyroid tissue of wild-type and *Thrb*$^{PV/PV}$*Pten*$^{+/-}$ mice. A. Hierarchical clustering analysis of the differential gene expression in thyroid tissues of wild-type (n=4) and *Thrb*$^{PV/PV}$*Pten*$^{+/-}$ (n=4) mice. B. Bar graph show the number of differentially altered total genes (2,322), up-regulated genes (1,062), and down-regulated genes (1,260) in thyroid tumors of *Thrb*$^{PV/PV}$*Pten*$^{+/-}$ mice compared with wild-type mice. C. Bar plots show the most consistent hallmark pathways of immune related target genes in thyroid tumors of *Thrb*$^{PV/PV}$*Pten*$^{+/-}$ mice (*P*<0.05 and fold change >2).

ated genes (*il15ra, il17re, irak3,* and *il1rl*), and chemokines (*Ccl21, Cxcl12, Ccr2,* and *Cxcl15*) were decreased in thyroid tumors of *Thrb*$^{PV/PV}$*Pten*$^{+/-}$ mice. We further validated the array data using RT-qPCR. Consistent with gene array data, mRNA expression profiling showed that *kit* was decreased 74% in the thyroid tumors of *Thrb*$^{PV/PV}$*Pten*$^{+/-}$ mice compared with *wild-type* mice (**Figure 3A**, panel a). The expression of *ly96* was decreased 64% (**Figure 3A**, panel b), and anti-inflammation related genes such as *CD163* and *Ephx2* were decreased 83% and 57% in the thyroid tumors of *Thrb*$^{PV/PV}$*Pten*$^{+/-}$ mice compared with wild-type mice, respectively (**Figure 3A**, panels c and d). The expressions of *il15* and *ccr2 were* decreased 80% and 61% in the thyroid tumors of *Thrb*$^{PV/PV}$*Pten*$^{+/-}$ mice compared with wild-type mice, respectively (**Figure 3A**, panels e and f).

**Table 2** shows the up-regulated immune-related genes in thyroid tumors of *Thrb*$^{PV/PV}$*Pten*$^{+/-}$ mice compared with wild-type. The changes ranged from a high of 19.85-fold down to 2.07-fold. We grouped these genes into three categories as in **Table 1**: Inflammation regulatory genes (5 genes were detected), interleukin-related genes (6 genes were found), and chemokines (6 genes were identified).

We selected genes for validation based on their functions related to inflammation. RT-qPCR data showed a significant increase in the expression of inflammatory mediators [such as *Ptgs1* (3.1-fold), *Sphk1* (7.5-fold), *Spp1* (OPN,

**Table 1.** Down-regulated immune-related genes in thyroid tumors of *Thrb$^{PV/PV}$Pten$^{+/-}$*

| | Gene | Gene name | Fold change |
|---|---|---|---|
| Inflammation-regulatory genes | Kit | KIT Proto-Oncogene Receptor Tyrosine Kinase | -10.02 |
| | Ly96 | Lymphocyte Antigen 96 | -4.31 |
| | Cd163 | CD163 antigen | -3.56 |
| | Ephx2 | Epoxide Hydrolase 2 | -4.19 |
| Interleukins | IL15 | Interleukin 15 | -4.48 |
| | Il15ra | Interleukin 15 receptor, alpha chain | -2.92 |
| | Il18 | Interleukin 18 | -2.24 |
| | Il17re | Interleukin 17 receptor E | -2.06 |
| | Irak3 | Interleukin-1 receptor-associated kinase 3 | -2.83 |
| | Il1r1 | Interleukin 1 receptor, type I | -5.39 |
| Chemokines | Ccl21a | Chemokine (C-C motif) ligand 21A | -2.21 |
| | Ccl21b | Chemokine (C-C motif) ligand 21B | -5.84 |
| | Ccl21c | Chemokine (C-C motif) ligand 21C | -2.72 |
| | Cxcl12 | Chemokine (C-X-C motif) ligand 12 | -3.33 |
| | Ccr2 | Chemokine (C-C motif) receptor 2 | -8.26 |
| | Cxcl15 | Chemokine (C-X-C motif) ligand 15 | -6.24 |

4.9-fold), *Chil1* (9.8-fold), *Tnfrsf18* (9.4-folds), *IL6* (7.5-fold), and *Ccl12* (3.2-fold)] in thyroid tumors of *Thrb$^{PV/PV}$Pten$^{+/-}$* mice (**Figure 3B**).

To further understand how those inflammatory regulators are modulated in human thyroid cancer patients, we used gene expression profiles from The Cancer Genome Atlas (TCGA) data (**Figure 3C**). Gene expression data from 509 thyroid cancer patients showed increased expression in the following genes (the fold increases are shown in parentheses): *SPHK1* (2.6), *SPP1* (2.8), *TNFRSF18* (3.9), *IL1RAP* (5.4), *CXCL17* (17), and *CHI3L* (17). TCGA data also showed decreased expression of *KIT* (91%), *EPHX2* (20%), *IL15* (20%), and *CCR2* (10%) in thyroid cancer patients as compared with normal healthy subjects. The concordance in the altered expression patterns of the genes listed above between thyroid cancer patients and thyroid tumors of *Thrb$^{PV/PV}$Pten$^{+/-}$* mice clearly shows the relevance and validity of the differentially expressed genes uncovered in the thyroid tumors of *Thrb$^{PV/PV}$Pten$^{+/-}$* mice. Taken together, these results suggest that increased inflammation in thyroid tumor microenvironment promotes thyroid carcinogenesis of *Thrb$^{PV/PV}$Pten$^{+/-}$* mice.

*Increased expression of osteopontin (OPN) and OPN-related inflammatory targets in thyroid tumors of Thrb$^{PV/PV}$Pten$^{+/-}$ mice*

To understand how increased infiltration of inflammatory monocytes (see **Figure 1B**) and altered expression of inflammatory-related genes (**Tables 1** and **2**) could contribute to thyroid carcinogenesis, we sought to identify key regulators impacting tumor progression. Among the pro-inflammatory mediators that were highly regulated in thyroid tumors listed in **Table 2**, secreted phosphoprotein 1 (SPP1, also known as osteopontin [OPN]) encoded by the *Spp1* gene caught our attention. OPN is a secreted protein present in body fluids and tissues. OPN, when bound to its receptor, integrin β1, regulates signaling cascades affecting adhesion, migration, invasion, chemotaxis, and cell survival [24, 25]. A variety of cells and tissues express OPN, including the bone, vasculature, kidney, inflammatory cells, and numerous secretory epithelia [26, 27]. Normal physiological roles of OPN include the regulation of immune functions, vascular remodeling, wound repair, and developmental processes [28]. OPN also is expressed in many cancers, and elevated levels in tumors and blood from patients are associated with poor prognosis [29, 30]. Within a tumor mass, OPN is expressed in both the tumor cells and cellular components of the tumor microenvironment such as macrophages and stromal cells [31]. The main role of OPN during inflammation is eliciting functional responses in leucocytes and inducing cytokine secretion, to direct the immune response [32, 33]. The critical roles of OPN in cancer and inflammation prompted us to focus our study on understanding how OPN mediates inflammation in thyroid cancer.

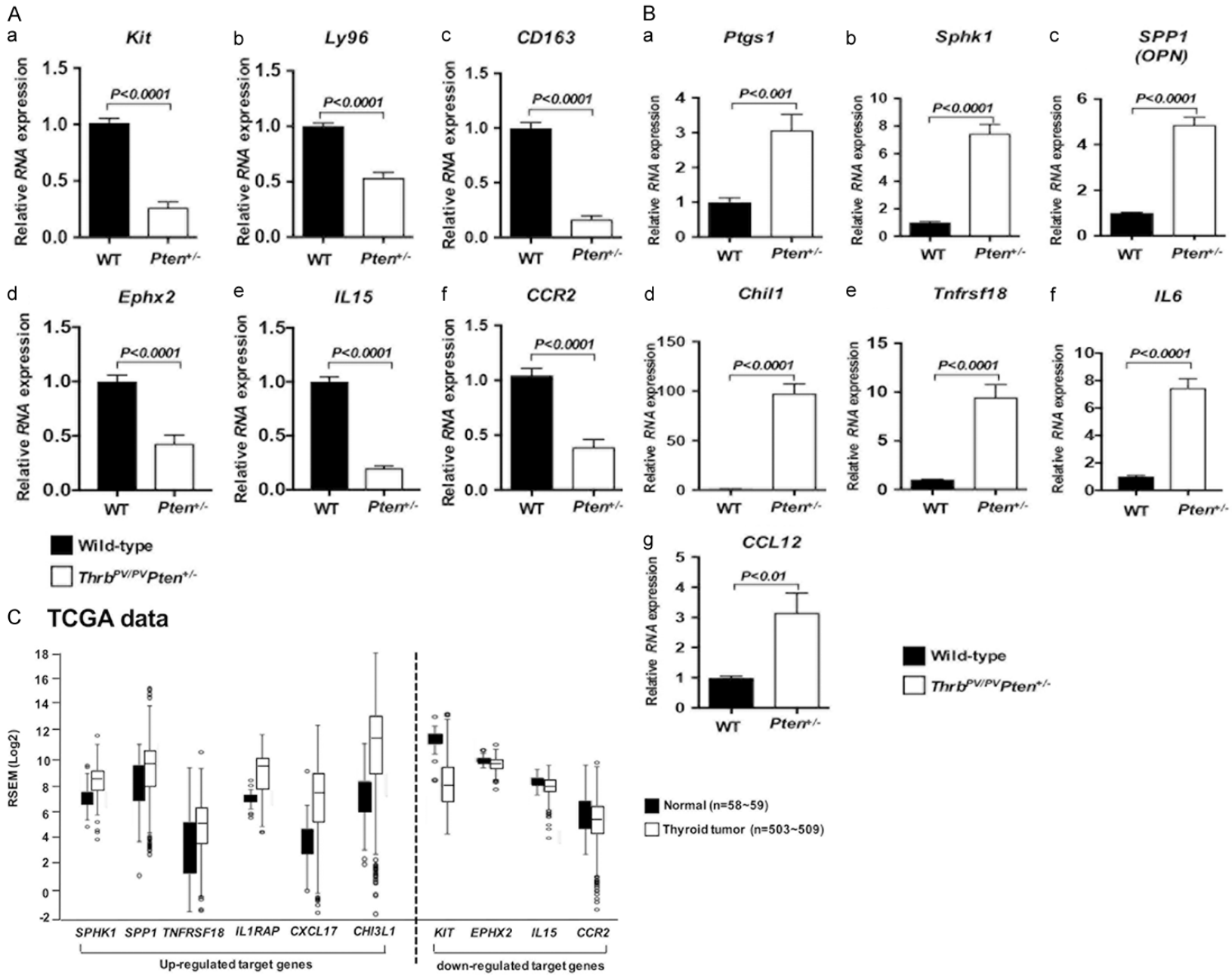
A
a
Kit
b
Ly96
c
CD163
d
Ephx2
e
IL15
f
CCR2
Relative RNA expression
P<0.0001
WT
Pten+/-
Wild-type
ThrbPV/PVPten+/-
B
a
Ptgs1
b
Sphk1
c
SPP1 (OPN)
d
Chil1
e
Tnfrsf18
f
IL6
g
CCL12
P<0.001
P<0.01
C
TCGA data
RSEM (Log2)
SPHK1
SPP1
TNFRSF18
IL1RAP
CXCL17
CHI3L1
KIT
EPHX2
IL15
CCR2
Up-regulated target genes
down-regulated target genes
Normal (n=58~59)
Thyroid tumor (n=503~509)

**Figure 3.** Alteration of inflammation-related genes in thyroid tumors of *Thrb$^{PV/PV}$Pten$^{+/-}$* mice. A. qPCR results of down-regulated inflammation modulators for *kit* (a), *Ly96* (b), *CD163* (c), *Ephx2* (d), *IL15* (e), and *CCR2* (f) in thyroid tumors of *Thrb$^{PV/PV}$Pten$^{+/-}$* mice (n=4) compared with wild-type mice (n=4). The mRNA level of each gene was normalized to the *GAPDH (glyceraldehyde-3-phosphate dehydrogenase)* mRNA level. Values are means ± SEM. The *P* values are indicated. B. qPCR results of up-regulated inflammation modulators for *Ptgs1* (a), *Sphk1* (b), *Spp1 (OPN)* (c), *Chil1* (d), *Tnfrsf18* (e), *Il6* (f), and *Ccl12* (g) in thyroid tumors of *Thrb$^{PV/PV}$Pten$^{+/-}$* mice (n=4) compared with wild-type mice (n=4). The mRNA level of each gene was normalized to the *GAPDH* mRNA level. Values are means ± SEM. The *P* values are indicated. C. Expression profile analysis of TCGA data to indicate up-regulated genes (*SPHK1, SPP1*, *TNFRSF18, IL1RAP*, *CXCL17,* and *CHI3L1*) and down-regulated genes (*KIT, EPHX2, IL15,* and *CCR2*) in normal thyroid (n=58 to ~59) and thyroid tumor from patients (n=503 to ~509).

**Table 2.** Up-regulated immune-related genes in thyroid tumors of *Thrb$^{PV/PV}$Pten$^{+/-}$*

| | Gene | Gene name | Fold change |
|---|---|---|---|
| Inflammation-regulatory genes | Ptgs1 | Prostaglandin-Endoperoxide Synthase 1 | 19.85 |
| | Sphk1 | Sphingosine Kinase 1 | 12.46 |
| | Spp1 | Secreted Phosphoprotein 1, Osteopontin (OPN) | 8.26 |
| | Chil1 | Chitinase-like (mouse), Chitinase 3-like (CHI3L1, Human) | 4.09 |
| | Tnfrsf18 | TFN Receptor Superfamily Member 18 | 7.9 |
| Interleukins | Il6 | Interleukin 6 | 2.13 |
| | Il10rb | Interleukin 10 receptor, beta | 2.07 |
| | Il1rap | Interleukin 1 receptor accessory protein | 2.71 |
| | Il24 | Interleukin 24 | 2.46 |
| | Nfil3 | Nuclear factor, interleukin 3, regulated | 4.22 |
| | Il4ra | Interleukin 4 receptor, alpha | 3.12 |
| Chemokines | Cxcr4 | Chemokine (C-X-C motif) receptor 4 | 2.44 |
| | Cxcl17 | Chemokine (C-X-C motif) ligand 17 | 15.14 |
| | Ccl12 | Chemokine (C -C motif) ligand 12 | 2.32 |
| | Cc18 | Chemokine (C -C motif) ligand 8 | 2.79 |
| | Cxcr4 | Chemokine (C-X-C motif) receptor 4 | 2.44 |
| | Ackr3 | Atypical chemokine receptor 3 | 2.14 |

Western blot analysis showed that the protein abundance of OPN was significantly increased in thyroid tumors of *Thrb$^{PV/PV}$Pten$^{+/-}$* mice. The full length form of OPN (**Figure 4A**, panel a) and the matrix metalloproteases (MMP) cleaved form of OPN (**Figure 4A**, panel b) were significantly increased in thyroid tumors of *Thrb$^{PV/PV}$Pten$^{+/-}$* mice (**Figure 4A**, panels a and b, lanes 4-6) compared with wild-type control (**Figure 4A**, panels a and b, lanes 1-3). Quantitative analysis indicated that the full length OPN and MMP cleaved OPN were increased 1.5-fold (**Figure 4B**, panel a) and 4.8-fold (**Figure 4B**, panel b), respectively. Extracellular OPN functions through its interaction with multiple cell surface receptors, such as integrin β1 [34-36], leading to the activation of PI3K-AKT [37] and NF-κB signaling. We found that integrin β1 levels were increased 3.3-fold in thyroid tumors of *Thrb$^{PV/PV}$Pten$^{+/-}$* mice (**Figure 4A**, panel c and quantification data shown in **Figure 4B**, panel c).

To assess the activation of AKT and NF-κB signaling, we examined protein levels of p-AKT and p65. p65 is typically involved in the body's inflammatory response as a part of the NF-κB signaling pathway. We showed that p-AKT and p65 protein levels were increased 3.1-fold and 2.2-fold in thyroid tumors of *Thrb$^{PV/PV}$Pten$^{+/-}$* mice, respectively (**Figure 4A**, panels d and f, and quantitation shown in **Figure 4B**, panels d and e). COX-2 expression induced by osteopontin stimulated NF-κB signaling cascade [38]. We found the expression of COX-2 was significantly increased in thyroid tumors of *Thrb$^{PV/PV}$Pten$^{+/-}$* mice (**Figure 4A**, panel g; 2.6-fold increase shown in **Figure 4B**, panel f). Consistently, we found that protein levels of TGF-β1 and TNF-α were increased 2.2-fold and

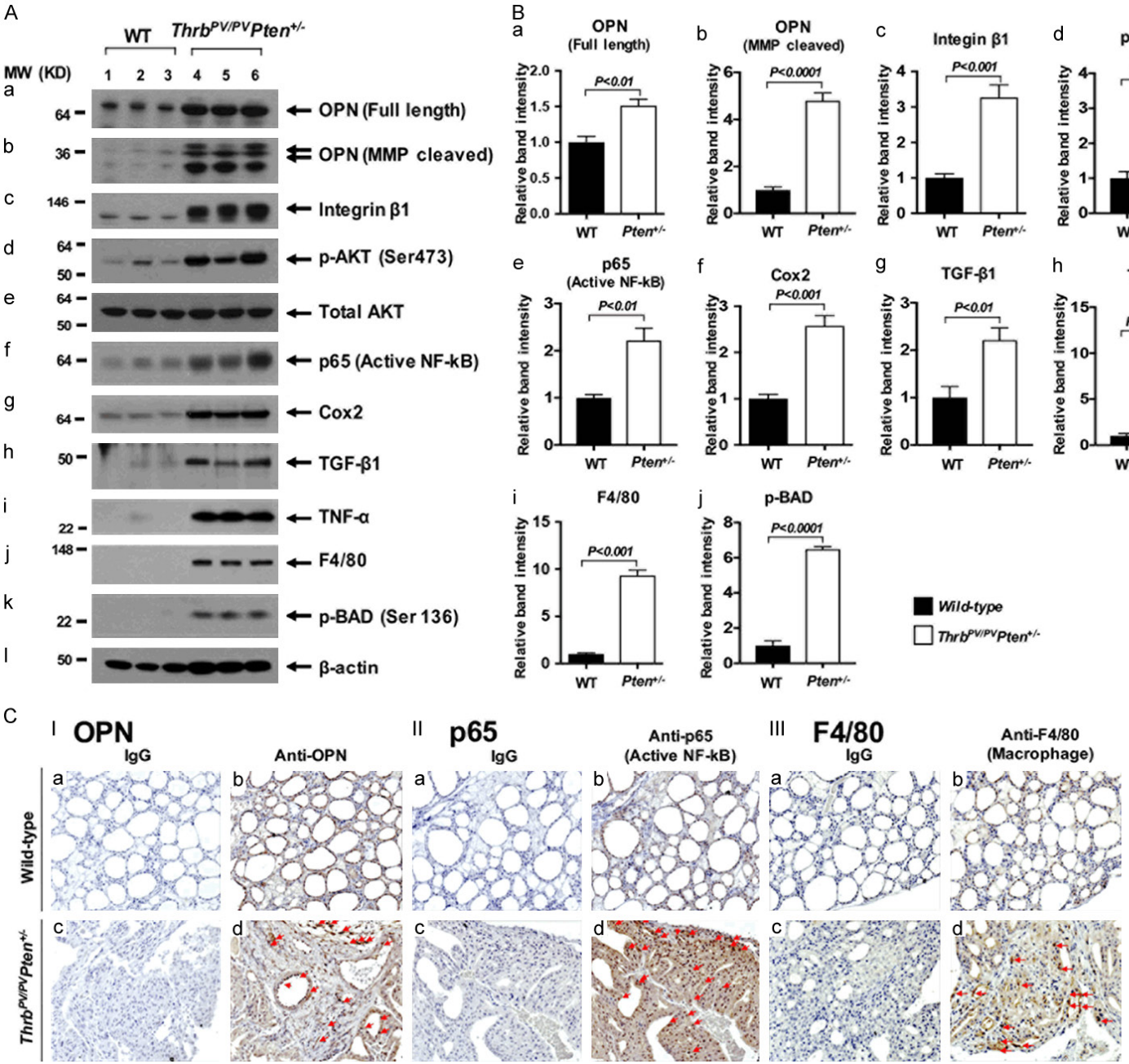
A
WT
ThrbPV/PVPten+/-
MW (KD)
1 2 3 4 5 6
a 64 OPN (Full length)
b 36 OPN (MMP cleaved)
c 146 Integrin β1
d 64 50 p-AKT (Ser473)
e 64 50 Total AKT
f 64 p65 (Active NF-kB)
g 64 Cox2
h 50 TGF-β1
i 22 TNF-α
j 148 F4/80
k 22 p-BAD (Ser 136)
l 50 β-actin
B
a OPN (Full length) P<0.01
b OPN (MMP cleaved) P<0.0001
c Integin β1 P<0.001
d p-AKT P<0.01
e p65 (Active NF-kB) P<0.01
f Cox2 P<0.001
g TGF-β1 P<0.01
h TNF-α P<0.001
i F4/80 P<0.001
j p-BAD P<0.0001
Relative band intensity
WT
Pten+/-
Wild-type
ThrbPV/PVPten+/-
C
I OPN
IgG
Anti-OPN
II p65
IgG
Anti-p65 (Active NF-kB)
III F4/80
IgG
Anti-F4/80 (Macrophage)
Wild-type
ThrbPV/PVPten+/-

**Figure 4.** Expression of OPN-related inflammatory targets in thyroid tumors of *Thrb*$^{PV/PV}$*Pten*$^{+/-}$ mice. (A) Western blot analysis for OPN (Full length, a), MMP cleaved-OPN (b), Integrin β1 (c), pAKT (d), total AKT (e), p65 (f), Cox 2 (g), TGF-β1 (h), TNF-α (i), F4/80 (j), p-BAD (k), and β-actin (l) in the thyroid tissue of wild-type and *Thrb*$^{PV/PV}$*Pten*$^{+/-}$ mice. β-actin used as a loading control (n=3-6 for each group). (B) The band intensities from western blot analysis detected in (A) were quantified by Image J analysis. OPN (Full length, a), MMP cleaved OPN (b), Integrin β1 (c), ratio of pAKT to total AKT (d), p65 (e), Cox 2 (f), TGF-β1 (g), TNF-α (h), F4/80 (i), and p-BAD (j). All band intensities were normalized using β-actin as a loading control. Values are shown as means ± SEM. The *P* values are indicated. (C) Immuno-histochemical analysis for OPN (I), p65 (II), and F4/80 (III) was carried out in the thyroid sections from wild-type (b in I-III) and *Thrb*$^{PV/PV}$*Pten*$^{+/-}$ mice (d in I-III). The representative positively stained cells are marked by arrows (d in I-III). The negative control panels using IgG are shown in the corresponding panels (a and c in I-III).

10.3-fold, respectively, in thyroid tumors of *Thrb*$^{PV/PV}$*Pten*$^{+/-}$ mice (**Figure 4A**, panels h and l, quantitation shown in **Figure 4B**, panels g and h). Importantly, we further showed increased expression of macrophage marker F4/80 in thyroid tumors of *Thrb*$^{PV/PV}$*Pten*$^{+/-}$ mice (**Figure 4A**, panel j). Quantitative analysis showed a 9.3-fold increase in F4/80 protein levels in thyroid tumors of *Thrb*$^{PV/PV}$*Pten*$^{+/-}$ mice (**Figure 4B**, panel i). In addition, we further examined the protein level of p-BAD (**Figure 4A**, panel k). BAD is a pro-apoptosis inducer. However, when phosphorylated at serine residues by several protein kinases such as AKT, p-BAD is sequestered in the cytosol through interaction with the cytosolic anchorage protein 14-3-3, resulting in the attenuation of its pro-apoptotic activity [39]. Consistent with the increased activity of p-AKT (see panel d, **Figure 4A**), we found that the protein level of p-BAD (Ser136) was increased 6.5-fold to increase the survival of tumor cells of *Thrb*$^{PV/PV}$*Pten*$^{+/-}$ mice (**Figure 4B**, panel i).

In addition to the determination of protein levels by western blotting, we examined the protein levels of the key molecules OPN, p65, and F4/80 by immuno-histochemical analysis (IHC). As shown in **Figure 4C**, increased OPN (panel I-d), p65 (panel II-d), and F4/80 (panel III-d) elevated protein levels in thyroid tissues of *Thrb*$^{PV/PV}$*Pten*$^{+/-}$ mice compared with wild-type mice (panels I-b, II-b and III-b). Taken together, these results indicated that increased OPN led to the activated downstream signaling to increase immune-inflammatory key regulators during thyroid carcinogenesis of *Thrb*$^{PV/PV}$*Pten*$^{+/-}$ mice.

## Discussion

The link of inflammation to cancers has long been recognized. A notable example is that patients with inflammatory bowel disease are at high risk of developing colon cancer [40]. The incidence of thyroid cancer, particularly the well-differentiated type, is known to increase in autoimmune thyroid disease such as Hashimoto's thyroiditis [41, 42]. Thyroid cancer was reported to frequently infiltrate with inflammatory cells such as lymphocytes, macrophages, dendritic cells, and mast cells. However, the roles of these infiltrated inflammatory cells in thyroid carcinogenesis have not been clearly understood. In the present studies, using a preclinical mouse model of follicular thyroid cancer (*Thrb*$^{PV/PV}$*Pten*$^{+/-}$ mice), we aimed to discern whether inflammation occurred during thyroid carcinogenesis and how inflammation could impact cancer progression.

We found that thyroid tumors were highly infiltrated with inflammatory monocytes (**Figure 1B**), while blood and bone marrow were unaffected. Global gene expression profiling identified differentially expressed genes highly enriched with altered expression of key inflammatory-related genes, interleukins, and chemokines (**Tables 1** and **2**). Further, we elucidated that OPN was a key driver in the immune-inflammatory response during thyroid carcinogenesis. Thus, the present studies have provided the direct molecular evidence to support the epidemiological observations and, importantly, shed new light on how inflammation could contribute to thyroid cancer progression.

It is important to highlight the key functional roles of OPN uncovered in the present studies in the cause-effect relationship of immune-inflammatory and thyroid cancer.

Consistent with the reports in other cancers [29], we found that the expression of OPN was highly induced during thyroid carcinogenesis. Concurrently, integrin β1, a receptor for OPN,

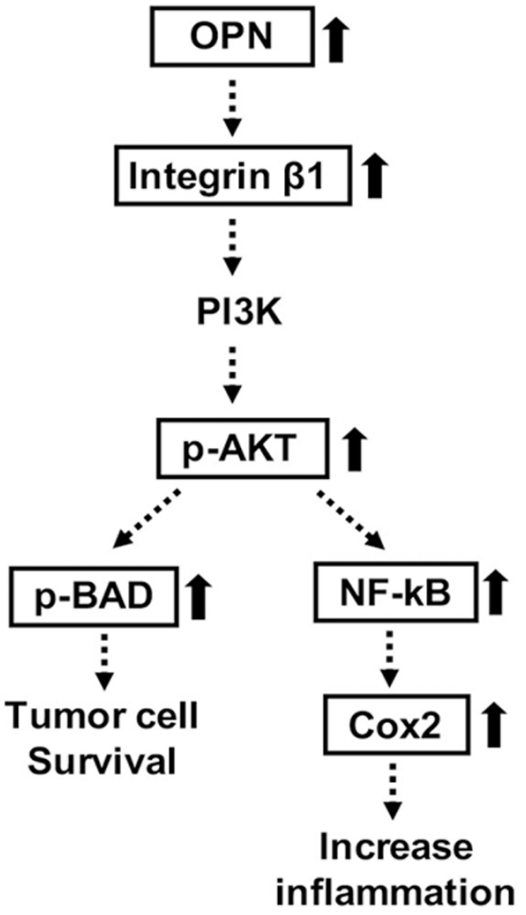


**Figure 5.** A proposed molecular model of the OPN-integrin β1-PI3K-AKT signaling in immune-inflammatory response in thyroid tumors of *Thrb*$^{PV/PV}$*Pten*$^{+/-}$ mice. OPN and its receptor, integrin β1, were highly increased in thyroid tumors of *Thrb*$^{PV/PV}$*Pten*$^{+/-}$ mice. Concordantly, AKT and NF-κB were significantly elevated in thyroid tumors of *Thrb*$^{PV/PV}$*Pten*$^{+/-}$ mice. The down-stream effectors of AKT and NF-κB pathways, p-BAD and Cox2, were significantly increased to elevate tumor cells survival and inflammation in thyroid tumors of *Thrb*$^{PV/PV}$*Pten*$^{+/-}$ mice.

was also elevated in thyroid tumors of *Thrb*$^{PV/PV}$*Pten*$^{+/-}$ mice (see **Figure 4A** and **4B**). The elevated OPN-integrin β1 led to the activation of downstream signaling via PI3K-AKT and NF-κB pathways to elevate Cox2 to increase inflammation. The activated OPN-integrin β-AKT signaling resulted in the suppression of pro-apoptotic activity of pBAD to promote survival of thyroid tumor cells (see **Figure 5**). The critical role of OPN functions elucidated in the present studies raised the possibility that OPN could be a potential molecular target as a novel treatment modality in thyroid cancer via modulating immune-inflammatory responses.

In the *Thrb*$^{PV/PV}$ mouse, there are two genetic alterations: the first is mutation of thyroid hormone receptor β (TRβPV); the second is the deletion of one allele of the *Pten* gene. While the first has yet to be found in thyroid cancer patients, the second is known as a genetic lesion that contributes to human thyroid cancer. However, it is important to point out that one of the functional consequences of TRβ mutations is the over-activation of PI3K-AKT signaling in the *Thrb*$^{PV/PV}$ mouse model [43, 44]. Further, PI3K-AKT signaling has been identified as a molecular target in thyroid cancer in the *Thrb*$^{PV/PV}$ mouse model [45]. The functional consequence of overactivation of PI3K-AKT as a result of TRβPV mutation is relevant in thyroid cancer. Activation of PI3K-AKT pathways play a pivotal role in the development of human thyroid cancer [46-48]. In the present study, we used the *Thrb*$^{PV/PV}$*Pten*$^{+/-}$ mouse in which the deletion of one allele of the *Pten* gene further drives the PI3K-AKT signaling, leading to a more aggressive follicular thyroid cancer than that in the *Thrb*$^{PV/PV}$ mouse [14]. The relevance of this *Thrb*$^{PV/PV}$*Pten*$^{+/-}$ mouse model for studying immune-inflammatory responses in thyroid cancer is evident in that the altered expression patterns of many critical inflammatory-related genes identified by gene expression profiling in the present study were also found in the TCGA database (see **Figure 3C**). Thus, the *Thrb*$^{PV/PV}$*Pten*$^{+/-}$ mouse could serve as a preclinical mouse model to test potential targets (e.g., OPN identified in the present studies) via altered immune-inflammatory responses for treatment of thyroid cancer.

## Acknowledgements

This research was supported by the Intramural Research Programs of the Center for Cancer Research of the National Cancer Institute, National Institutes of Health.

## Disclosure of conflict of interest

None.

**Address correspondence to:** Dr. Sheue-Yann Cheng, Laboratory of Molecular Biology, Cancer and Inflammation Program, Center for Cancer Research, National Cancer Institute, Building 37, Rm: 5128A2, 37 Convent Drive MSC 4264, Bethesda, Maryland 20892-4264, USA. Tel: 240-760-7828; E-mail: chengs@mail.nih.gov

## References


[1] Landa I, Ibrahimpasic T, Boucai L, Sinha R, Knauf JA, Shah RH, Dogan S, Ricarte-Filho JC, Krishnamoorthy GP, Xu B, Schultz N, Berger MF, Sander C, Taylor BS, Ghossein R, Ganly I and Fagin JA. Genomic and transcriptomic hallmarks of poorly differentiated and anaplastic thyroid cancers. J Clin Invest 2016; 126: 1052-1066.

[2] Pozdeyev N, Gay LM, Sokol ES, Hartmaier R, Deaver KE, Davis S, French JD, Borre PV, LaBarbera DV, Tan AC, Schweppe RE, Fishbein L, Ross JS, Haugen BR and Bowles DW. Genetic analysis of 779 advanced differentiated and anaplastic thyroid cancers. Clin Cancer Res 2018; 24: 3059-3068.

[3] Coussens LM and Werb Z. Inflammation and cancer. Nature 2002; 420: 860-867.

[4] Balkwill F and Mantovani A. Inflammation and cancer: back to virchow? Lancet 2001; 357: 539-545.

[5] Mantovani A, Allavena P, Sica A and Balkwill F. Cancer-related inflammation. Nature 2008; 454: 436-444.

[6] Colotta F, Allavena P, Sica A, Garlanda C and Mantovani A. Cancer-related inflammation, the seventh hallmark of cancer: links to genetic instability. Carcinogenesis 2009; 30: 1073-1081.

[7] Matsubayashi S, Kawai K, Matsumoto Y, Mukuta T, Morita T, Hirai K, Matsuzuka F, Kakudoh K, Kuma K and Tamai H. The correlation between papillary thyroid carcinoma and lymphocytic infiltration in the thyroid gland. J Clin Endocrinol Metab 1995; 80: 3421-3424.

[8] Modi J, Patel A, Terrell R, Tuttle RM and Francis GL. Papillary thyroid carcinomas from young adults and children contain a mixture of lymphocytes. J Clin Endocrinol Metab 2003; 88: 4418-4425.

[9] Yano Y, Shibuya H, Kitagawa W, Nagahama M, Sugino K, Ito K and Ito K. Recent outcome of graves' disease patients with papillary thyroid cancer. Eur J Endocrinol 2007; 157: 325-329.

[10] French JD, Weber ZJ, Fretwell DL, Said S, Klopper JP and Haugen BR. Tumor-associated lymphocytes and increased FoxP3+ regulatory T cell frequency correlate with more aggressive papillary thyroid cancer. J Clin Endocrinol Metab 2010; 95: 2325-2333.

[11] Ugolini C, Basolo F, Proietti A, Vitti P, Elisei R, Miccoli P and Toniolo A. Lymphocyte and immature dendritic cell infiltrates in differentiated, poorly differentiated, and undifferentiated thyroid carcinoma. Thyroid 2007; 17: 389-393.

[12] Ryder M, Ghossein RA, Ricarte-Filho JC, Knauf JA and Fagin JA. Increased density of tumor-associated macrophages is associated with decreased survival in advanced thyroid cancer. Endocr Relat Cancer 2008; 15: 1069-1074.

[13] Caillou B, Talbot M, Weyemi U, Pioche-Durieu C, Al Ghuzlan A, Bidart JM, Chouaib S, Schlumberger M and Dupuy C. Tumor-associated macrophages (TAMs) form an interconnected cellular supportive network in anaplastic thyroid carcinoma. PLoS One 2011; 6: e22567.

[14] Guigon CJ, Zhao L, Willingham MC and Cheng SY. PTEN deficiency accelerates tumour progression in a mouse model of thyroid cancer. Oncogene 2009; 28: 509-517.

[15] Park JW, Han CR, Zhao L, Willingham MC and Cheng SY. Inhibition of STAT3 activity delays obesity-induced thyroid carcinogenesis in a mouse model. Endocr Relat Cancer 2016; 23: 53-63.

[16] Park S, Willingham MC, Qi J and Cheng SY. Metformin and JQ1 synergistically inhibit obesity-activated thyroid cancer. Endocr Relat Cancer 2018; 25: 865-877.

[17] Zhu X, Zhao L, Park JW, Willingham MC and Cheng SY. Synergistic signaling of KRAS and thyroid hormone receptor beta mutants promotes undifferentiated thyroid cancer through MYC up-regulation. Neoplasia 2014; 16: 757-769.

[18] Kim J and Bae JS. Tumor-associated macrophages and neutrophils in tumor microenvironment. Mediators Inflamm 2016; 2016: 6058147.

[19] Hume DA. The mononuclear phagocyte system. Curr Opin Immunol 2006; 18: 49-53.

[20] Auffray C, Sieweke MH and Geissmann F. Blood monocytes: development, heterogeneity, and relationship with dendritic cells. Annu Rev Immunol 2009; 27: 669-692.

[21] Ingersoll MA, Spanbroek R, Lottaz C, Gautier EL, Frankenberger M, Hoffmann R, Lang R, Haniffa M, Collin M, Tacke F, Habenicht AJ, Ziegler-Heitbrock L and Randolph GJ. Comparison of gene expression profiles between human and mouse monocyte subsets. Blood 2010; 115: e10-19.

[22] Jakubzick C, Gautier EL, Gibbings SL, Sojka DK, Schlitzer A, Johnson TE, Ivanov S, Duan Q, Bala S, Condon T, van Rooijen N, Grainger JR, Belkaid Y, Ma'ayan A, Riches DW, Yokoyama WM, Ginhoux F, Henson PM and Randolph GJ. Minimal differentiation of classical monocytes as they survey steady-state tissues and transport antigen to lymph nodes. Immunity 2013; 39: 599-610.

[23] Hiltbrunner S, Larssen P, Eldh M, Martinez-Bravo MJ, Wagner AK, Karlsson MC and Gabrielsson S. Exosomal cancer immunotherapy is independent of MHC molecules on exosomes. Oncotarget 2016; 7: 38707-38717.

[24] Denhardt DT, Noda M, O'Regan AW, Pavlin D and Berman JS. Osteopontin as a means to cope with environmental insults: regulation of inflammation, tissue remodeling, and cell survival. J Clin Invest 2001; 107: 1055-1061.
[25] Agnihotri R, Crawford HC, Haro H, Matrisian LM, Havrda MC and Liaw L. Osteopontin, a novel substrate for matrix metalloproteinase-3 (stromelysin-1) and matrix metalloproteinase-7 (matrilysin). J Biol Chem 2001; 276: 28261-28267.
[26] Higashibata Y, Sakuma T, Kawahata H, Fujihara S, Moriyama K, Okada A, Yasui T, Kohri K, Kitamura Y and Nomura S. Identification of promoter regions involved in cell- and developmental stage-specific osteopontin expression in bone, kidney, placenta, and mammary gland: an analysis of transgenic mice. J Bone Miner Res 2004; 19: 78-88.
[27] Takahashi F, Takahashi K, Shimizu K, Cui R, Tada N, Takahashi H, Soma S, Yoshioka M and Fukuchi Y. Osteopontin is strongly expressed by alveolar macrophages in the lungs of acute respiratory distress syndrome. Lung 2004; 182: 173-185.
[28] Anborgh PH, Mutrie JC, Tuck AB and Chambers AF. Role of the metastasis-promoting protein osteopontin in the tumour microenvironment. J Cell Mol Med 2010; 14: 2037-2044.
[29] Rittling SR and Chambers AF. Role of osteopontin in tumour progression. Br J Cancer 2004; 90: 1877-1881.
[30] Fedarko NS, Jain A, Karadag A, Van Eman MR and Fisher LW. Elevated serum bone sialoprotein and osteopontin in colon, breast, prostate, and lung cancer. Clin Cancer Res 2001; 7: 4060-4066.
[31] Tuck AB, O'Malley FP, Singhal H, Harris JF, Tonkin KS, Kerkvliet N, Saad Z, Doig GS and Chambers AF. Osteopontin expression in a group of lymph node negative breast cancer patients. Int J Cancer 1998; 79: 502-508.
[32] Weber GF, Zawaideh S, Hikita S, Kumar VA, Cantor H and Ashkar S. Phosphorylation-dependent interaction of osteopontin with its receptors regulates macrophage migration and activation. J Leukoc Biol 2002; 72: 752-761.
[33] Bruemmer D, Collins AR, Noh G, Wang W, Territo M, Arias-Magallona S, Fishbein MC, Blaschke F, Kintscher U, Graf K, Law RE and Hsueh WA. Angiotensin II-accelerated atherosclerosis and aneurysm formation is attenuated in osteopontin-deficient mice. J Clin Invest 2003; 112: 1318-1331.
[34] Bayless KJ and Davis GE. Identification of dual alpha 4beta1 integrin binding sites within a 38 amino acid domain in the N-terminal thrombin fragment of human osteopontin. J Biol Chem 2001; 276: 13483-13489.
[35] Smith LL, Cheung HK, Ling LE, Chen J, Sheppard D, Pytela R and Giachelli CM. Osteopontin N-terminal domain contains a cryptic adhesive sequence recognized by alpha9beta1 integrin. J Biol Chem 1996; 271: 28485-28491.
[36] Katagiri YU, Sleeman J, Fujii H, Herrlich P, Hotta H, Tanaka K, Chikuma S, Yagita H, Okumura K, Murakami M, Saiki I, Chambers AF and Uede T. CD44 variants but not CD44s cooperate with beta1-containing integrins to permit cells to bind to osteopontin independently of arginine-glycine-aspartic acid, thereby stimulating cell motility and chemotaxis. Cancer Res 1999; 59: 219-226.
[37] Lin YH and Yang-Yen HF. The osteopontin-CD44 survival signal involves activation of the phosphatidylinositol 3-kinase/Akt signaling pathway. J Biol Chem 2001; 276: 46024-46030.
[38] Jain S, Chakraborty G and Kundu GC. The crucial role of cyclooxygenase-2 in osteopontin-induced protein kinase C alpha/c-Src/IkappaB kinase alpha/beta-dependent prostate tumor progression and angiogenesis. Cancer Res 2006; 66: 6638-6648.
[39] Yan J, Zhang H, Xiang J, Zhao Y, Yuan X, Sun B and Lin A. The BH3-only protein BAD mediates TNFalpha cytotoxicity despite concurrent activation of IKK and NF-kappaB in septic shock. Cell Res 2018; 28: 701-718.
[40] Fornaro R, Caratto M, Caratto E, Caristo G, Fornaro F, Giovinazzo D, Sticchi C, Casaccia M and Andorno E. Colorectal cancer in patients with inflammatory bowel disease: the need for a real surveillance program. Clin Colorectal Cancer 2016; 15: 204-212.
[41] Noureldine SI and Tufano RP. Association of hashimoto's thyroiditis and thyroid cancer. Curr Opin Oncol 2015; 27: 21-25.
[42] Pisanu A, Piu S, Cois A and Uccheddu A. Coexisting Hashimoto's thyroiditis with differentiated thyroid cancer and benign thyroid diseases: indications for thyroidectomy. Chir Ital 2003; 55: 365-372.
[43] Furuya F, Hanover JA and Cheng SY. Activation of phosphatidylinositol 3-kinase signaling by a mutant thyroid hormone beta receptor. Proc Natl Acad Sci U S A 2006; 103: 1780-1785.
[44] Furuya F, Guigon CJ, Zhao L, Lu C, Hanover JA and Cheng SY. Nuclear receptor corepressor is a novel regulator of phosphatidylinositol 3-kinase signaling. Mol Cell Biol 2007; 27: 6116-6126.
[45] Furuya F, Lu C, Willingham MC and Cheng SY. Inhibition of phosphatidylinositol 3-kinase delays tumor progression and blocks metastatic spread in a mouse model of thyroid cancer. Carcinogenesis 2007; 28: 2451-2458.

[46] Xing M. Genetic alterations in the phosphatidylinositol-3 kinase/Akt pathway in thyroid cancer. Thyroid 2010; 20: 697-706.
[47] Wang Y, Hou P, Yu H, Wang W, Ji M, Zhao S, Yan S, Sun X, Liu D, Shi B, Zhu G, Condouris S and Xing M. High prevalence and mutual exclusivity of genetic alterations in the phosphatidylinositol-3-kinase/akt pathway in thyroid tumors. J Clin Endocrinol Metab 2007; 92: 2387-2390.
[48] Landa I and Knauf JA. Mouse models as a tool for understanding progression in braf (V600E)-driven thyroid cancers. Endocrinol Metab (Seoul) 2019; 34: 11-22.

**Table S1.** Primer list for RT-qPCR

| | Forward primer | Reverse primer |
|---|---|---|
| *Kit* | 5'-TCATCGAGTGTGATGGGAAA-3' | 5'-GGTGACTTGTTTCAGGCACA-3' |
| *Ly96* | 5'-CTTTTCGACGCTGCTTTCTC-3' | 5'-CCATGGCACAGAACTTCCTT-3' |
| *CD163* | 5'-CCTCCTCATTGTCTTCCTCCTGTG-3' | 5'-CATCCGCCTTTGAATCCATCTCTTG-3' |
| *Ephx2* | 5'-CTGGATACCCTGAAGGCAAA-3' | 5'-TGACGTCATTTGGATTGCAT-3' |
| *Il15* | 5'-GTGACTTTCATCCCAGTTGC-3' | 5'-TTCCTTGCAGCCAGATTCTG-3' |
| *Ccr2* | 5'-GCCAGGACAGTTACCTTTGG-3' | 5'-CGAAACAGGGTGTGGAGAAT-3' |
| *Ptgs1* | 5'-GTGCTGGGGCAGTGCTGGAG-3' | 5'-TGGGGCCTGAGTAGCCCGTG-3' |
| *Sphk1* | 5'-GGCTCTGCAGCTCTTCCAGAG-3' | 5'-CTCCTCTGCACACACCAGCTC-3' |
| *Spp1(OPN)* | 5'-AGCAAGAAACTCTTCCAAGCA-3' | 5'-GTGAGATTCGTCAGATTCATCCG-3' |
| *Chil1* | 5'-AGAGGCCCTGACTAGGAAGC-3' | 5'-GTGCACAGGAAAGGTTGGAT-3' |
| *Tnfrsf18* | 5'-GACGGTCACTGCAGACTTTG-3' | 5'-GCCATGACCAGGAAGATGAC-3' |
| *Il6* | 5'-CCTCTGGTCTTCTGGAGTACC-3' | 5'-ACTCCTTCTGTGACTCCAGC-3' |
| *Ccl12* | 5'-AGAATCACAAGCAGCCAGTGT-3' | 5'-ATCCAAGTGGTTTATGGAATTCTTAAC-3' |

**Table S2.** Antibody list for FACS analysis

| Antibody | Clone ID | Purpose | Manufacturer |
|---|---|---|---|
| CD3e | 145-2C11 | Lineage Depletion | Tonbo |
| CD19 | 1D3 | Lineage Depletion | Tonbo |
| NKp46 (CD335) | 29A1.4 | Lineage Depletion | Ebioscience |
| Ly6G (Gr-1) | 1A8 | Lineage Depletion | Tonbo |
| Sca-1 | D7 | Lineage Depletion | Biolegend |
| Ter119 | Ter119 | Lineage Depletion | Tonbo |
| Ly6C | HK1.4 | Sort | Biolegend |
| MHC-II | M5/114.15/2 | Sort | BD |
| cKit (CD117) | 2B8 | Sort | BD |
| CD115 | AFS98 | Sort | Biolegend |
| CD45 | 30-F11 | Sort | Ebioscience |